



P-wave tomography and origin of the Changbai intraplate volcano in Northeast Asia

Jianshe Lei*, Dapeng Zhao

Geodynamics Research Center, Ehime University, Matsuyama 790-8577, Japan

Received 15 July 2004; received in revised form 12 September 2004; accepted 9 December 2004
Available online 25 January 2005

Abstract

We present the first seismic image of the upper mantle beneath the active intraplate Changbai volcano in Northeast Asia determined by teleseismic travel time tomography. The data are measured at a new seismic network consisting of 19 portable stations and 3 permanent stations. Our results show a columnar low-velocity anomaly extending to 400-km depth with a P-wave velocity reduction of up to 3%. High velocity anomalies are visible in the mantle transition zone, and deep-focus earthquakes occur at depths of 500–600 km under the region, suggesting that the subducting Pacific slab is stagnant in the transition zone, as imaged clearly by global tomography. These results suggest that the intraplate Changbai volcano is not a hotspot like Hawaii but a kind of back-arc volcano related to the deep subduction and stagnancy of the Pacific slab under Northeast Asia.

© 2004 Elsevier B.V. All rights reserved.

Keywords: Changbai volcano; Intraplate volcanism; Subducted Pacific slab; Teleseismic travel time tomography

1. Introduction

In mainland China there are three active volcanoes: Wudalianchi and Changbai volcanoes in northeastern (NE) China, and Tengchong volcano in southern China. These three volcanoes are all active volcanoes, and have erupted many times in the history. For example, the Wudalianchi volcano erupted during 1719–1721 (Liu, 2000), the Tengchong volcano

erupted during 1465–1620 (Liu, 2000), and the Changbai volcano erupted six times in BC 1120, AD 1050, 1413, 1597, 1668, and 1702 (Simkin and Siebert, 1994). However, the origin of these intraplate volcanoes is still unclear.

Many researchers have used geological, geochemical, and geophysical approaches to study the Changbai volcano (e.g., Zhang and Tang, 1983; Zindler and Hart, 1986; Zhao, 1991; Basu et al., 1991; Zhang and O'Reilly, 1997; Fan et al., 1999a,b; Tang et al., 1999; Wang et al., 2003). Magnetotelluric soundings show that lower resistivity anomalies exist beneath the Changbai volcano in the crust (Tang et al., 1997, 2001). Seismic explosion experiments revealed low-

* Corresponding author. Tel.: +81 89 927 8257; fax: +81 89 927 8167.

E-mail addresses: leijs@sci.ehime-u.ac.jp (J. Lei), zhao@sci.ehime-u.ac.jp (D. Zhao).

velocity anomalies in the crust and upper mantle down to a depth of 40 km, suggesting the existence of magma chambers under the Changbai volcano (Zhang et al., 2002).

The Changbai volcano is also called Tianchi or Baitoushan volcano, which is located in the Changbai Mountains, close to the boundary between NE China and North Korea. Some researchers suggested that the Changbai volcano was originated via either accretion processes at the craton margin since Mesoproterozoic or due to subduction processes of the Pacific plate before the opening of the Japan Sea (e.g., Zhang and O'Reilly, 1997). Turcotte and Schubert (1982) assumed that it is a hotspot like Hawaii volcano, while Tatsumi et al. (1990) considered that it is a kind of back-arc volcano. The global tomographic models are still too rough to resolve the detailed structure and the origin of the Changbai intraplate volcanism.

With the recent installation of 19 portable seismic stations during the NE China seismic experiments (Wu and Hetland, 1999), a few studies have been made to investigate the structure under NE China. For example, receiver function techniques were applied to the data set recorded by the portable seismic network to study the crust structure and upper mantle discontinuities (Ai et al., 2003; Li and Yuan, 2003; Hetland et al., 2004). These studies showed that the crust is thicker and contains low-velocity anomalies beneath the Changbai volcano, and that the subducted Pacific slab is stagnating in the mantle transition zone beneath the volcano. It is also suggested that pieces of slab materials have penetrated into the lower mantle under NE Asia (Ai et al., 2003). However, no tomographic study has been made using this new data set. The availability of abundant teleseismic data recorded by this portable seismic network allows us to determine a 3-D velocity structure beneath the Changbai volcano to understand its origin.

In this study we have applied a tomographic method to relative travel time residuals from the teleseismic events recorded by the NE China seismic network and the permanent China Digital Seismic Network (CDSN) to determine a 3-D P-wave velocity structure of the crust and upper mantle beneath the Changbai volcano. Our tomographic results provide a new insight into the origin of the intraplate volcanism in NE Asia.

2. Data and method

Fig. 1a shows the distribution of seismic stations used in this study. The portable seismic network contains 19 broad-band seismic stations equipped with Guralp 3T three-component digital seismometers (Wu and Hetland, 1999; Hetland et al., 2004). In this work we also used the data from 3 permanent seismic stations, MDJ, HIA, and BJT from CDSN (Fig. 1a)

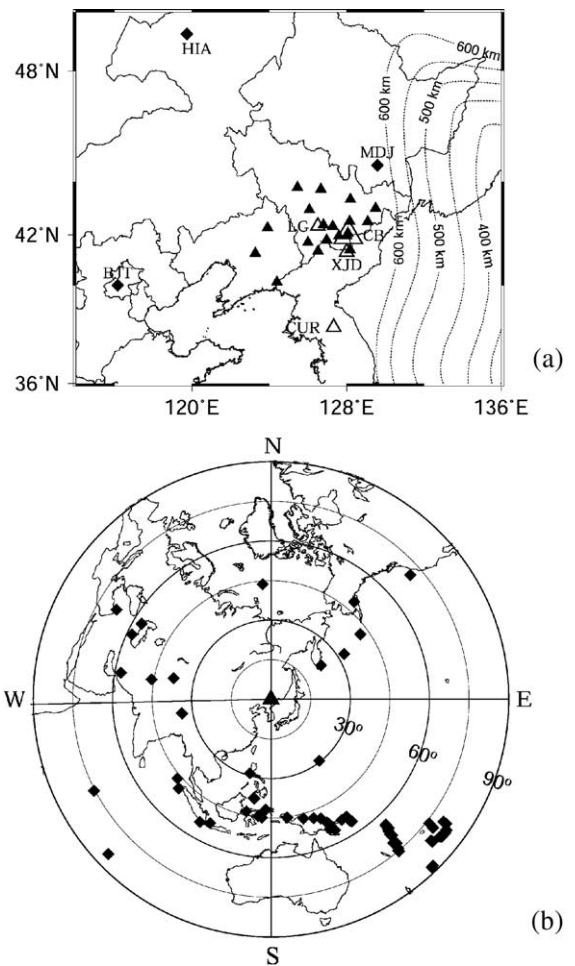


Fig. 1. (a) Locations of 19 portable seismic stations (▲) and 3 permanent stations (◆) used in this study. Open triangles denote the intraplate volcanoes. CB, Changbai; LG, Longgang; XJD, Xianjindao; CUR, Ch'uga-Ryong (Simkin and Siebert, 1994). The dotted lines show the depth contours of the Wadati-Benioff deep seismic zone (Gudmundsson and Sambridge, 1998). (b) Epicentral locations of the 68 teleseismic events (diamonds) used in this study. The triangle denotes the center of the NE China Seismic Network.

which are located adjacent to the portable seismic network and have data recordings since 1986. The 19 temporary seismic stations were located around the Changbai volcano and had been in operation from late June to September 1998, ten of which continued till April 1999 (for details see [Hetland et al., 2004](#)). The geometry of the subducting Pacific slab as estimated from the deep seismicity by [Gudmundsson and Sambridge \(1998\)](#) is also shown in [Fig. 1a](#).

We hand-picked P-wave arrival times from high-quality original seismograms ([Fig. 2](#)). The picking accuracy is estimated to be 0.1–0.2 s. The resulting data set contains 548 high-quality P arrival times from 68 teleseismic events. [Fig. 1b](#) shows the geographic locations of the 68 teleseismic events, which were relocated by R. Engdahl (see [Engdahl et al., 1998](#)). The magnitudes of these events are greater than M

4.8. The events selected have a good azimuthal coverage except in the Pacific Ocean and Russia. Except for one event in Kamchatka that has an epicentral distance of about 25°, all other events are located between 30° and 90° from the seismic network. The ray paths used in this study are shown in [Fig. 3](#).

We used the iasp91 1-D Earth model ([Kennett and Engdahl, 1991](#)) to calculate the theoretical P-wave travel times. They were corrected for the Earth’s ellipticity ([Dziewonski and Gilbert, 1976](#)). When calculating the travel times, we also determined the teleseismic ray paths between the hypocenter and receiver and found the intersection between the ray and the boundary planes of the modeling space. Then we used the 3-D ray tracer of [Zhao et al. \(1992\)](#) to determine the ray path between the intersection and

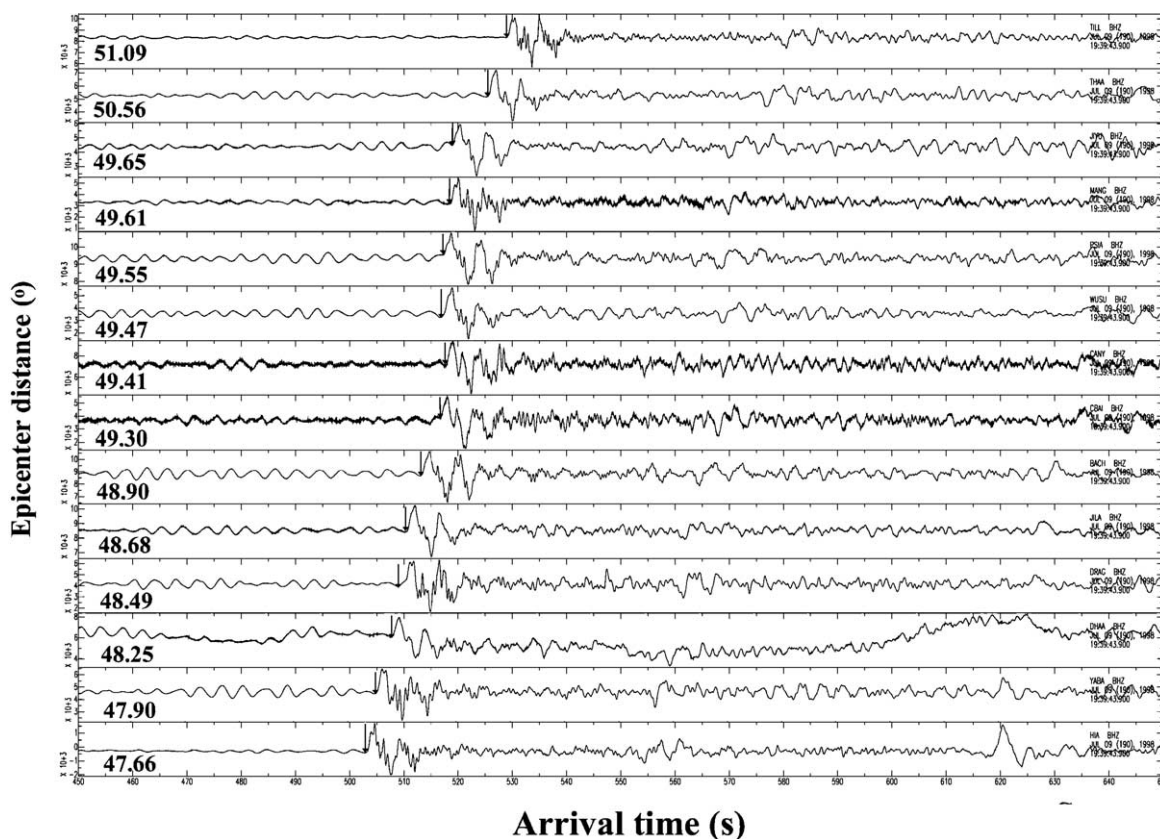


Fig. 2. An example showing the original seismograms recorded by the NE China Seismic Network and China Digital Seismic Network for an earthquake (Mw 6.2) occurred in South Alaska on July 9, 1998. The arrows show the P first arrivals we picked. The number on the left under each trace denotes the epicentral distance in degrees.

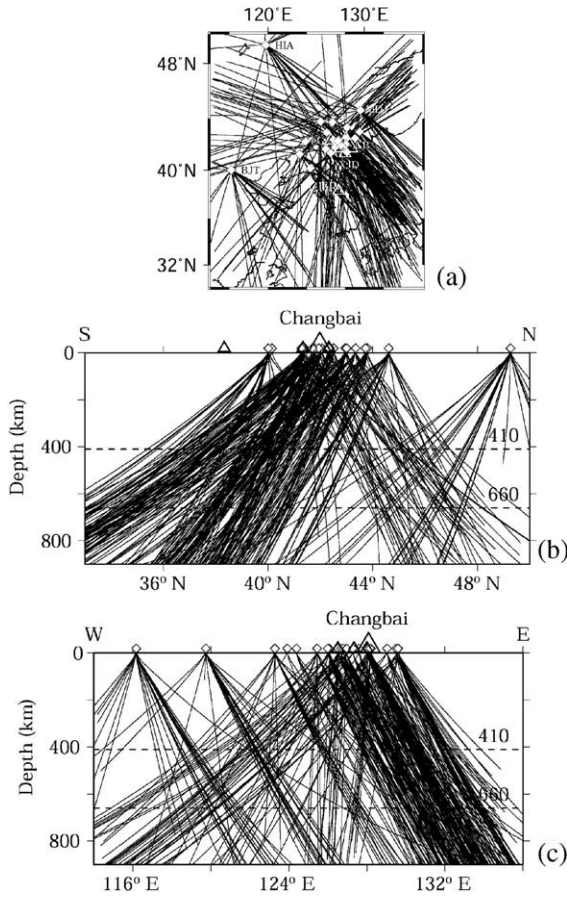


Fig. 3. Distribution of P rays used in this study in plane view (a) and in the north–south (b) and east–west (c) vertical cross-sections. Grey and white diamonds denote portable and permanent stations, respectively. Open triangles show the intraplate volcanoes.

the station. This 3-D ray tracer can calculate the travel times and ray paths efficiently and accurately, and can deal with a velocity model that contains velocity discontinuities of complex geometry and 3-D velocity variations everywhere in the model (for details, see Zhao et al., 1992; Zhao and Lei, 2004).

From the observed arrival times, travel time residual t_{ij} , from the j -th event to the i -th station, can be expressed as

$$t_{ij} = T_{ij}^{\text{OBS}} - T_{ij}^{\text{CAL}}, \quad (1)$$

where T_{ij}^{OBS} and T_{ij}^{CAL} are observed and calculated travel times, respectively. In order to minimize the effects of hypocenter mislocations, origin times, and

velocity heterogeneities outside the study area, relative travel time residuals r_{ij} are adopted in the tomographic inversion. From the Eq. (1), relative residuals r_{ij} are expressed as

$$r_{ij} = t_{ij} - t_j^m, \quad (2)$$

where $t_j^m = \frac{1}{n_j} \sum_{i=1}^{n_j} t_{ij}$ is the average residual, and n_j is the number of observations for the j -th event. From the Eq. (2), the average relative residual r_i^m at the i -th station can be expressed as

$$r_i^m = \frac{1}{k_i} \sum_{j=1}^{k_i} r_{ij}, \quad (3)$$

where k_i is the number of events observed by the i -th station.

Fig. 4 shows the distribution of the relative travel time residuals. There is a clear pattern that delayed arrivals appear at stations around the Changbai, Longgang, and Xianjindao volcanoes (Simkin and Siebert, 1994). At stations far from the Changbai volcano, they show early arrivals. Although some stations between the Changbai and Longgang volcanoes also show early arrivals, their amplitudes are much smaller than those far from the Changbai volcano (Fig. 4b). The maximum amplitudes of the early and delayed arrivals amount to ± 0.38 s. This distribution of the relative residuals simply indicates that low-velocity anomalies exist under the active intraplate volcanoes.

After calculating the relative travel time residuals, we used the tomographic method of Zhao et al. (1994) to determine the 3-D P-wave velocity (V_p) structure beneath the Changbai volcano. A 3-D grid was set up in the study area; the velocities at the grid nodes were taken as unknown parameters. The velocity at any point in the model was obtained by interpolating the velocities at the eight grid nodes surrounding that point. A conjugate gradient algorithm (Paige and Saunders, 1982) was used to invert the large and sparse system of observation equations.

3. Resolution analyses

A direct way to evaluate the resolution of a tomographic result is to calculate a set of travel

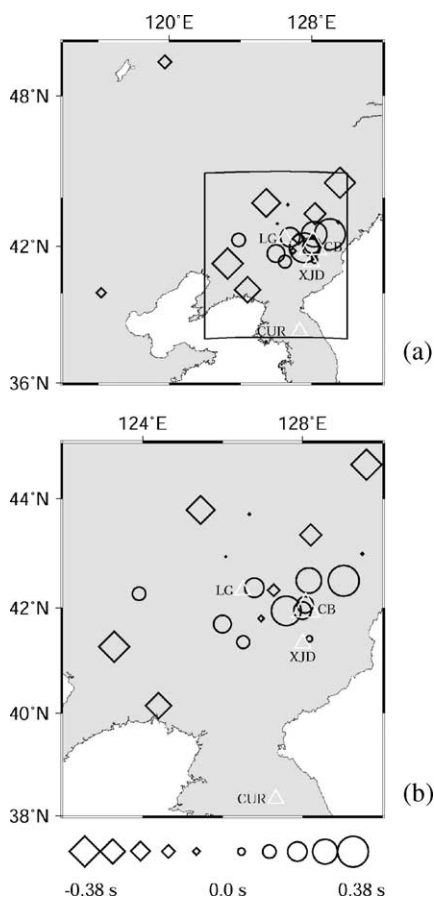


Fig. 4. (a) Distribution of P-wave relative travel time residuals at each of the 22 seismic stations. (b) An enlarged version of the box in (a). Early and delayed arrivals are shown in diamonds and circles, respectively. The scale for the residuals is shown at the bottom. The large triangle shows the Changbai volcano. The smaller triangles show three less prominent volcanoes in NE China and Korea.

time delays that result from tracing the corresponding rays through a synthetic structure as though they are data, and then to compare the inversion result with the initial synthetic structure. In the synthetic tests, the numbers of the stations, events, and ray paths are the same as those in the real data set. In this study we conducted two kinds of resolution tests to assess the adequacy of the ray coverage and evaluate the resolution. One is synthetic tests for examining the resolvability of the structure right beneath the Changbai volcano, the other is checkerboard resolution tests for evaluating the spatial resolution of tomographic

images in the entire study area. The checkerboard resolution test is just a special form of synthetic test. The only difference between them is in the input model. To make a checkerboard, positive and negative 3% velocity perturbations are assigned to 3-D grid nodes that are arranged in the modeling space, the image of which is straightforward and easy to remember. Therefore, by just seeing the image of the synthetic inversion of the checkerboard, one can easily understand where the resolution is good and where it is poor. In this study many such tests were performed by adopting different grid spacings. From our extensive resolution tests, we found that the optimal grid spacing for the tomographic inversion of our data set is $2^\circ \times 2^\circ$ in the horizontal directions. In this optimal model we put the grid nodes at depths of 10, 100, 300, 500, 700, and 900 km.

The results of five synthetic tests beneath the Changbai volcano are shown in Figs. 5 and 6. The first one is that slow velocity anomalies of up to -3% are put from the surface to 800-km depth in the initial model (Fig. 5a,c). The second is that slow anomalies of up to -3% are put from the surface to 400-km depth and fast anomalies of up to $+3\%$ are put from 400- to 800-km depth in the initial model (Fig. 5e,g). The third and fourth are that in the initial models slow anomalies of up to -3% are put from the surface to 200-km and 400-km depths, respectively (Fig. 6a,c). The fifth is that high velocity anomalies of $+3\%$ are put in the mantle transition zone in the initial model (Fig. 6e).

The corresponding output models are shown on the right panels of Figs. 5 and 6. The output models in the upper mantle have almost the same patterns as the input models though there are some differences between them in the amplitude. The images in the mantle transition zone have a lower resolution than those in the upper mantle, because the degree of ray crisscrossing below 400-km depth is not as good as that in the upper mantle.

We adopted two ways to present the results of the checkerboard resolution test (Figs. 7 and 8). One is the conventional way as shown on the left panels of Figs. 7 and 8. The open and solid circles show the inverted results of the slow and fast velocity anomalies assigned at the grid nodes in the

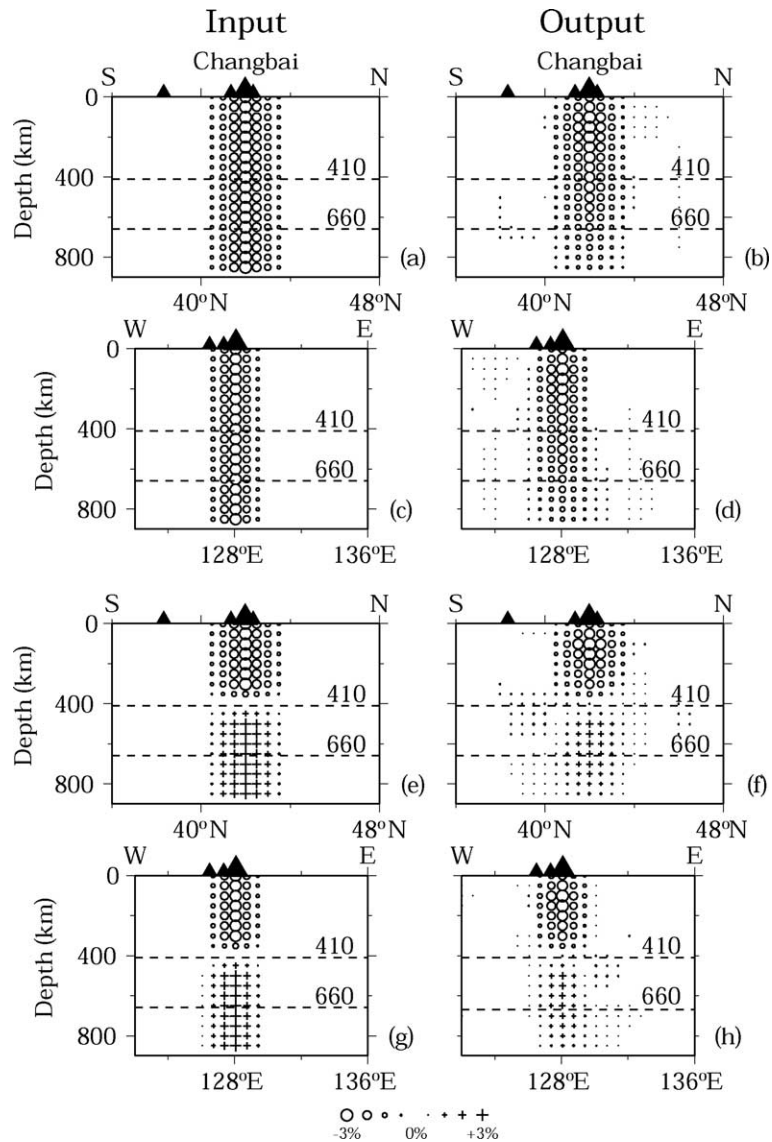


Fig. 5. Input models (left) and inverted results (right) of the synthetic tests for P-wave structure along the north–south (a, b, e, f) and east–west (c, d, g, h) vertical cross-sections (see text for details). Circles and crosses denote slow and fast velocities, respectively. The scale for circles and crosses is shown at the bottom. Solid triangles show the volcanoes. The two dashed lines denote the 410 and 660 km discontinuities. The locations of cross-sections are shown in the insert map of Fig. 10.

checkerboard test. Sometimes it is uneasy to discern if the checkerboard pattern is recovered correctly or not, in particular, for the edge parts of the study area. In order to better show the results of the checkerboard test, we adopted another way (Lei and Zhou, 2002) as shown on the right panels of Figs. 7 and 8. The stars denote the grid nodes where the

pattern of the input velocity anomalies is correctly recovered after the inversion, that is, fast anomalies in the input model are recovered to be fast, and slow ones in the input model are recovered to be slow after the inversion. On the contrary, crosses in Figs. 7 and 8 denote the grid nodes where the pattern of the input velocity anomalies is wrongly

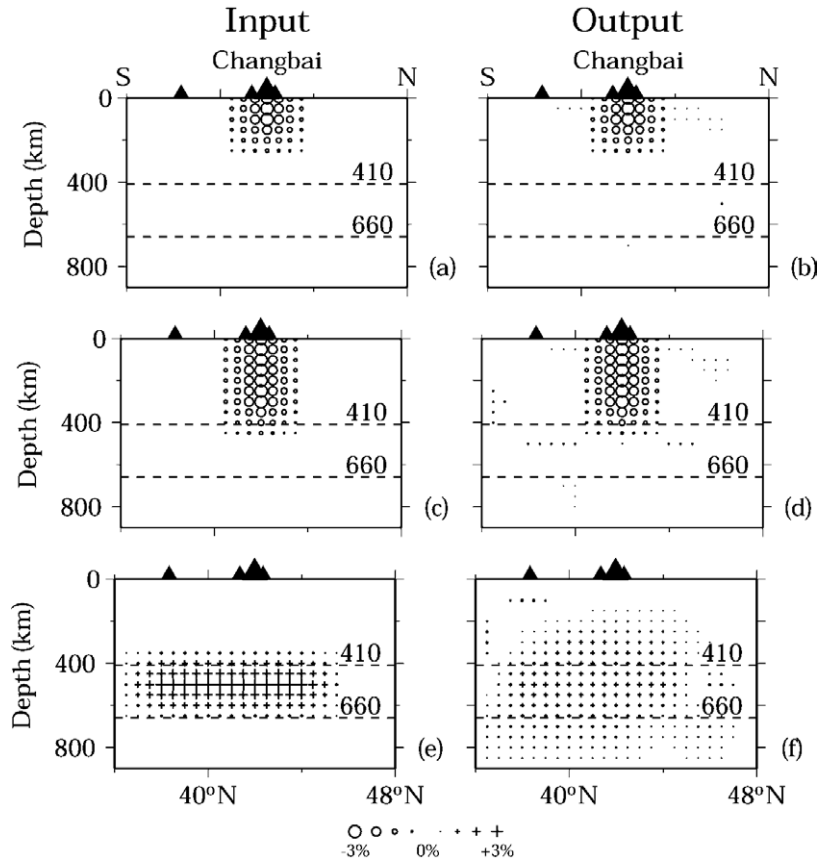


Fig. 6. The same as Fig. 5 but for other three synthetic tests.

recovered after the inversion. The size of the star and cross symbols denotes the ratio of the inverted amplitude of the velocity anomaly to the value of the input velocity anomaly. The stars with values of 100% show the grid nodes where the checkerboard model is recovered perfectly.

The shallower parts (10 km) of the study area have a lower resolution (Figs. 7 and 8) because the teleseismic rays do not crisscross well in the shallow crust (Fig. 3). This is usual for the teleseismic tomography. By using the star-cross way it is easy to find whether the grid nodes are recovered correctly or not at the depth of 10 km (Fig. 7a and b). As a whole the resolution in the upper mantle is better than that in the mantle transition zone and below (Figs. 7 and 8), being consistent with the results of the synthetic tests (Figs. 5 and 6).

4. Results

Figs. 9 and 10 show our final results. The V_p tomography shows a prominent low-velocity anomaly beneath the Changbai volcano at the shallow depth (10 km), and this anomaly elongates slightly westward and southward, which may be related to the existence of volcanoes to the west and south, such as the Longgang, Xianjindao, and Ch’Uga-Ryong volcanoes (Simkin and Siebert, 1994). Furthermore, it is visible that a NE oriented fault passes through the Changbai volcano and the center of the low-velocity zone. The fault may represent a fracture zone in the crust or the lithosphere, which may facilitate the magma ascent to the surface. Some shallow earthquakes occurred around the low velocity anomaly (Fig. 9a). The geometry of the slow anomaly changes greatly at 100-km depth. Its southern part is close to

the Ch’Uga-Ryong volcano (Fig. 9b). At 300-km depth, the slow anomaly is reduced in size and mainly concentrates beneath the Changbai, Longgang, and Xianjindao volcanoes. A slow anomaly is also visible beneath the Ch’Uga-Ryong volcano to the south (Fig. 9c). In the mantle transition zone (500-km depth) some high-velocity patches are visible and deep earthquakes occurred actively there (Fig. 9d). At 700-km depth high velocity anomalies are also visible

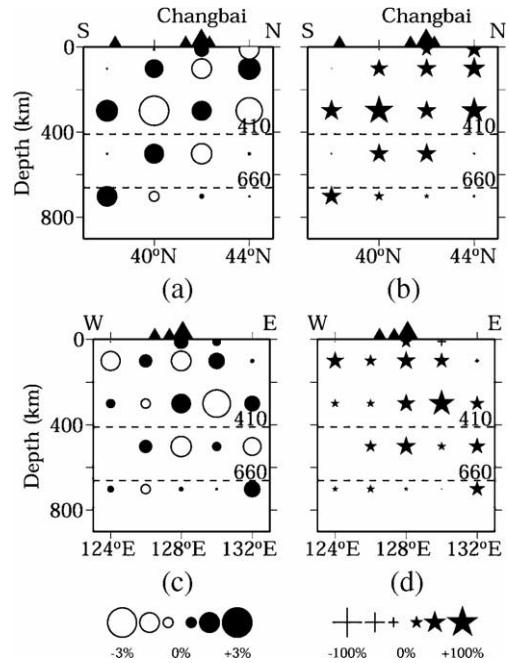
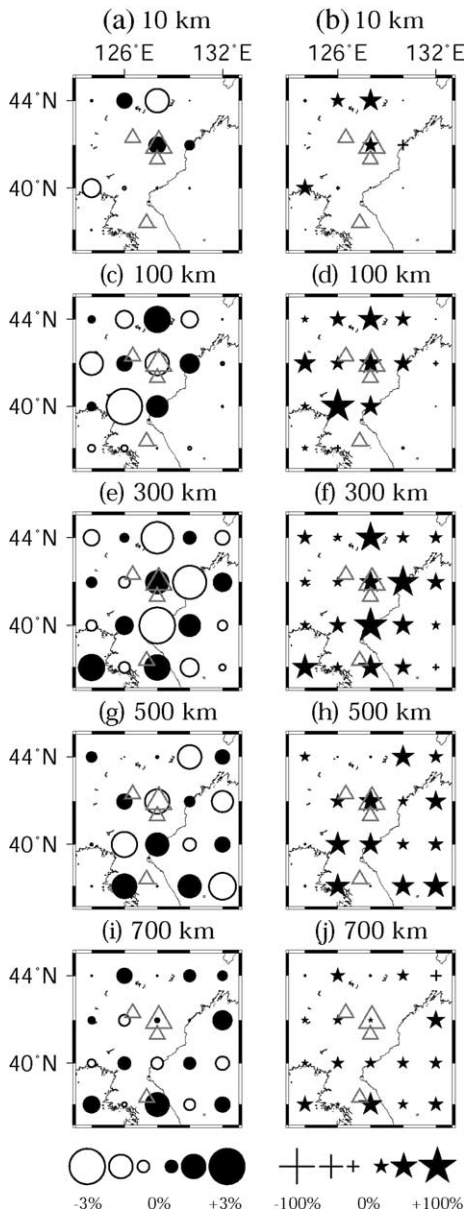


Fig. 8. The same as Fig. 7 but for vertical cross-sections along the north–south (a, b) and east–west (c, d) profiles. The dashed lines denote the 410 and 660 km discontinuities. Locations of the cross-sections are shown in the insert map of Fig. 10.

beneath the volcanoes (Fig. 9e). Receiver function analyses showed that the 660 km discontinuity is depressed by tens of kilometers due to the influence of the subducting Pacific slab under this region (Ai et al., 2003; Li and Yuan, 2003). Hence the high-velocity anomalies at 500- and 700-km depths in our tomographic images may show the subducted Pacific slab

Fig. 7. Results of a checkerboard resolution test for P-wave structure in plane views. The layer depth is shown above each map. Open triangles denote the four intraplate volcanoes. (Left) Open and solid circles show the inverted results of the slow and fast velocity anomalies at the grid nodes after the inversion. The velocity perturbation scale is shown at the bottom. (Right) Stars denote the grid nodes where the pattern of the input velocity anomalies is recovered correctly after the inversion, that is, fast anomalies in the input model are recovered to be fast, and slow ones in the input model are recovered to be slow after the inversion. While the crosses denote the grid nodes where the pattern of the input velocity anomalies is wrongly recovered after the inversion. The size of the star and cross symbols denotes the ratio of the inverted amplitude of the velocity anomaly to the value of the velocity anomaly in the input model. The stars with values of 100% show the grid nodes where the checkerboard pattern is recovered perfectly. The scale for the degree of recovery (stars and crosses) is shown at the bottom.

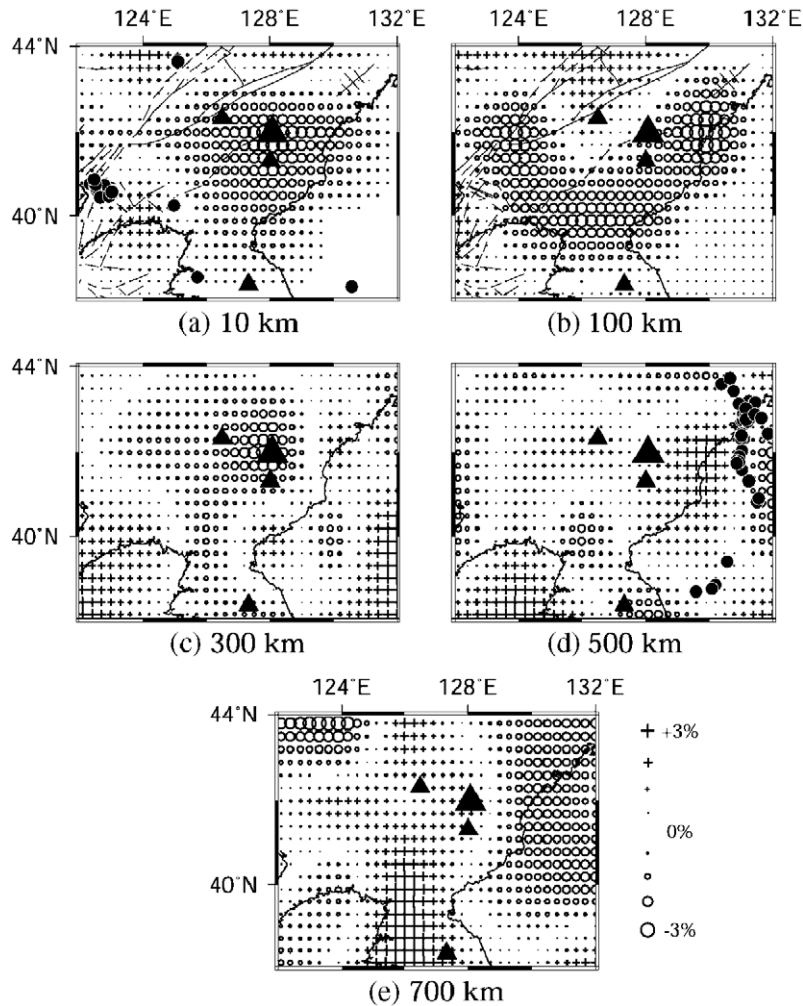


Fig. 9. P-wave velocity perturbations at (a) 10-km, (b) 100-km, (c) 300-km, (d) 500-km, and (e) 700-km depths. Open circle and cross denote low and high velocity anomalies, respectively. The velocity perturbation scale is shown beside (e). Solid triangles denote the volcanoes. Dots show the earthquakes within 100-km depth range of each layer. Thin lines in (a) and (b) denote faults.

that is stagnant in the mantle transition zone under NE Asia.

From the vertical cross-sections we can see that large slow anomalies of up to -3% are imaged with a diameter of about 200 km beneath the Changbai volcano (Fig. 10). These slow anomalies extend continuously down to 400-km depth, which look like an inclined cylinder. The complex geometry of the slow anomalies may be due to the existence of several intraplate volcanoes in the region as shown in the plane map. The mantle transition zone under the Changbai area generally exhibits fast anomalies

(Fig. 10a and b). The synthetic and checkerboard tests (Figs. 5–8) show that these main features are reliable. In particular, Fig. 6b and d show that the depth extent of these slow anomalies is not an artifact but a reliable feature.

In this study, as Allen et al. (2002) did, we also performed corrections for the crustal heterogeneity by adopting the 3-D crustal velocity model of Sun et al. (2004) for the Changbai region. This 3-D crustal model contains both lateral velocity variations in the crust and the uppermost mantle and depth variation of the Moho discontinuity. This model has a lower

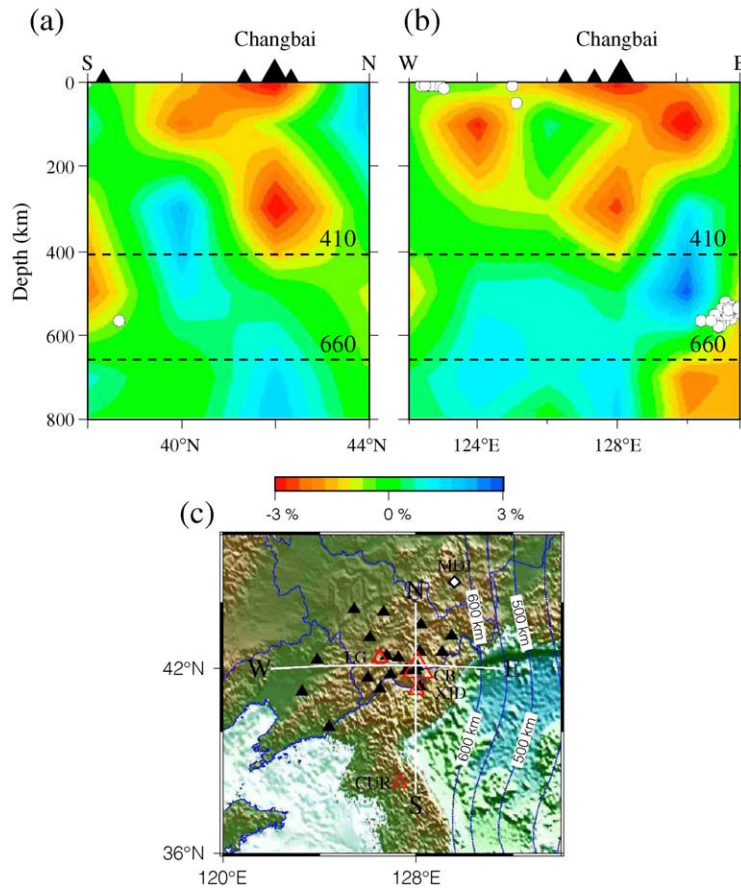


Fig. 10. North–south (a) and east–west (b) vertical cross-sections of P-wave velocity images. Red and blue colors denote low and high velocity anomalies, respectively. The velocity perturbation scale is shown below the cross-sections. Black triangles in (a) and (b) denote the volcanoes. White dots show the earthquakes within 100 km of the profiles. The two dashed lines denote the 410 and 660 km discontinuities. The locations of the cross-sections are shown in the insert map (c). Labelings in (c) are the same as those in Fig. 1a.

resolution but it is still better than other crustal models in this region (see Sun et al., 2004 for details). Fig. 11 shows the resulting images after the crustal correction. Comparing Figs. 10 and 11 we can find that both of the upper mantle models exhibit the same features: low-velocity anomalies extend down to about 400-km depth and high-velocity anomalies are visible in the mantle transition zone and below.

5. Discussion and conclusions

A global tomography model (Zhao, 2004) shows better images of the subducting slab in the mantle transition zone (Fig. 12) because many seismic

phases (P, pP, PP, PcP, and Pdiff) have been used in the inversion. However, the global model only shows a blurred slow anomaly in the upper mantle beneath the Changbai volcano because of the large grid spacing ($5^\circ \times 5^\circ$) adopted in the global tomographic inversion.

Although there exist some differences, the global and regional models show a similar structure feature of the upper mantle and the transition zone under NE Asia (Figs. 10–12). A very slow anomaly exists in the upper mantle right beneath the Changbai volcano, right above the stagnant Pacific slab in the mantle transition zone. This result is also quite similar to the images under the Fiji–Tonga region where the back-arc volcanoes in Fiji and Lau spreading center are

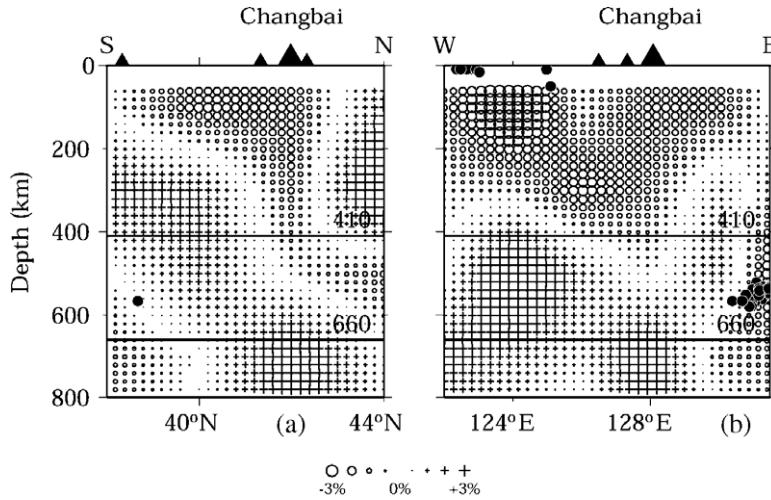


Fig. 11. The same as Fig. 10 but for the results after the crustal travel time correction. Open circle and cross denote low and high velocity anomalies, respectively. Black triangles denote the volcanoes. Dots denote earthquakes occurred within 100 km of the profile. The two thick lines denote the 410 and 660 km discontinuities. The velocity perturbation scale is shown at the bottom. Locations of the cross-sections are shown in the insert map of Fig. 10.

located above very slow anomalies in the mantle wedge right above the subducting Tonga slab (Zhao et al., 1997).

There are basically four types of volcanism on Earth: mid-ocean ridge volcanism, subduction zone volcanism, hotspots associated with mantle plumes,

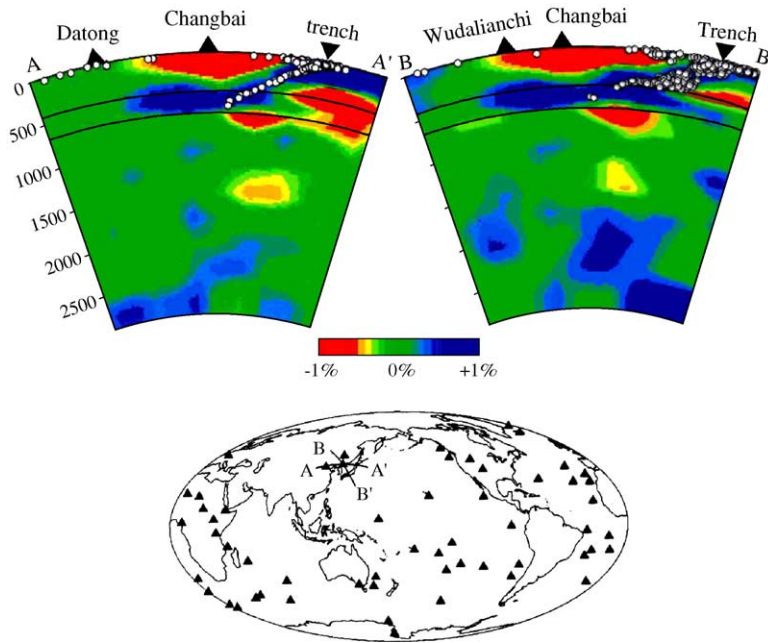


Fig. 12. Vertical cross-sections of P-wave velocity images determined by a global tomographic inversion (Zhao, 2004). Locations of the cross-sections are shown in the insert map. Red and blue colors denote low and high velocities, respectively. The velocity perturbation scale is shown below the cross-sections. Black triangles on the top of the cross-sections denote volcanoes. The reversed triangle shows the location of the Japan Trench. White dots show the earthquakes within 150 km of the profiles. The two solid lines denote the 410 and 660 km discontinuities. The triangles in the insert map show hotspot volcanoes except those in NE Asia.

and intraplate volcanism related to lithospheric fracture and asthenospheric injection (Tatsumi et al., 1990; Yin, 2000; Zhao, 2001a). Apparently, the Changbai volcanism does not belong to the first type. Because the stagnant Pacific slab exists beneath NE

Asia, the origin of the Changbai volcano differs from that of the Hawaii, Iceland, and Eifel volcanoes which are considered to be hotspots overlying mantle plumes (e.g., Wolfe et al., 1997; Ritter et al., 2001; Zhao, 2001a; Keyser et al., 2002).

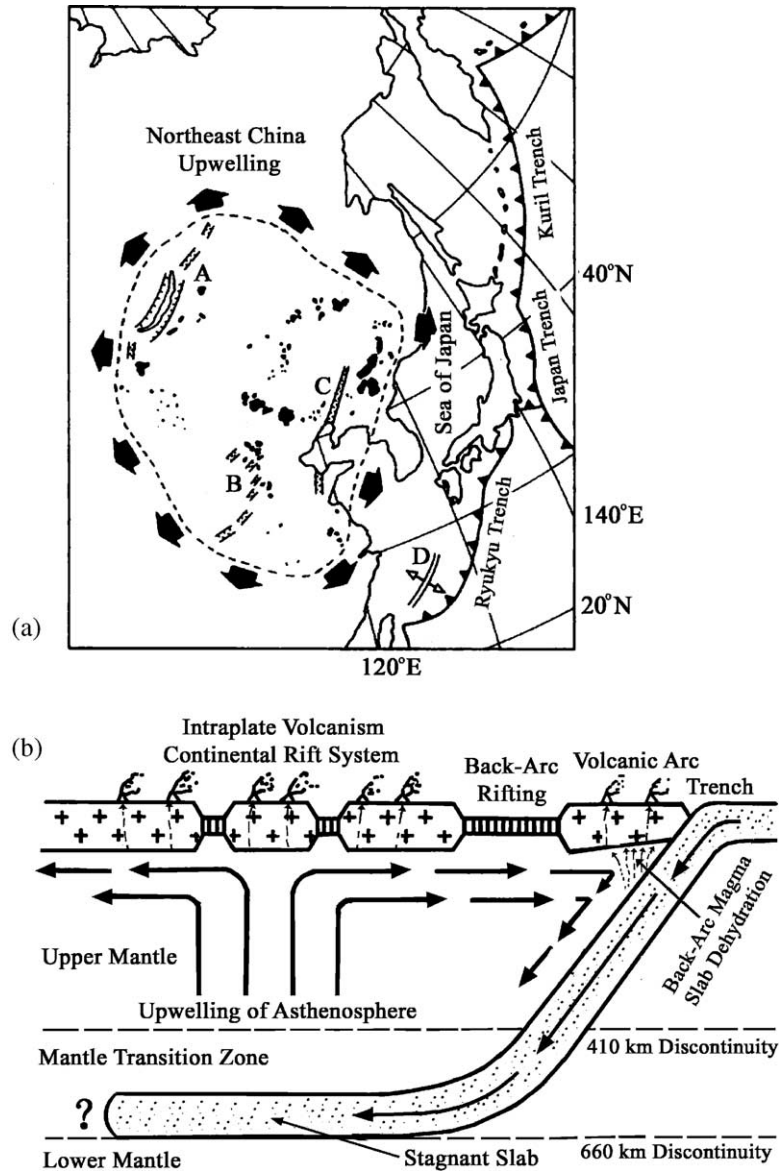


Fig. 13. (a) Tectonic features on the surface in Northwest Pacific and NE Asia. Black patches denote the Cenozoic basalts. A, Baikal rift; B, Shanxi graben; C, Tancheng-Lujiang fault zone; D, Okinawa trough. (b) A schematic east-west vertical section showing the upper mantle structure beneath NE Asia. The subducting Pacific slab becomes stagnant in the mantle transition zone. The deep dehydration process of the slab and convective circulation process in the mantle wedge cause upwellings of high-temperature asthenospheric materials, leading to the formation of the continental rift system as well as intraplate volcanoes in NE Asia (modified from Tatsumi et al., 1990).

Some plate boundary zones are considered as broad deformation zones, rather than narrow boundaries assumed at the beginning of the plate tectonics theory (Stein and Freymueller, 2002). For example, the continental collision between the India and Eurasian plates has resulted in the Tibet plateau of several thousand kilometers wide. The Changbai volcano is located about 1000 km away from the Japan Trench where the subducting Pacific slab enters the mantle, and it lies above the stagnant Pacific slab in the mantle transition zone. These results suggest that the Northwest Pacific subduction zone is a very broad deformation zone and the deep subduction of the Pacific slab influences the seismic and volcanic activity in the interior of the Eurasian continental plate far beyond the traditional plate boundary areas such as the island arcs and continental margins alone.

Because the very old Pacific plate is subducting beneath NE Asia at a rapid rate (7–10 cm/year), dehydration reactions may not be completely finished at the shallow depths (100–200 km) of the mantle. Hydrous Mg–Si minerals in the subducting Pacific slab may continue to release fluids through dehydration reactions at the depths of the mantle transition zone. This scenario has been demonstrated in the experimental petrology and other studies (Thompsons, 1992; Staudigel and King, 1992). Recent mineral physics experiments also showed that the mantle transition zone contains several times more water than the other portions of the mantle and the transition zone could be an important water reservoir in the Earth's interior (Inoue et al., 2004). Deep dehydration reactions have also been found in the Tonga subducting zone (Zhao et al., 1997).

These results indicate that the active intraplate volcanoes in NE Asia are not hotspots but a sort of back-arc volcanoes which are closely related to the subduction processes of the Pacific slab. Slow velocity anomalies in the back-arc region are generally associated with the back-arc magmatism and volcanism caused by the deep dehydration process of the subducting slab and convective circulation process of the mantle wedge (Zhao et al., 1997; Zhao, 2001b). These processes may lead to a large-scale upwelling of the asthenospheric materials under NE Asia and cause intraplate volcanism and continental rift systems in the region. Tatsumi et al. (1990) first invoked the

asthenospheric injection to explain the formation of the Wudalianchi and Changbai volcanoes, but they did not consider the stagnant Pacific slab under the region because such a slab structure was unknown at that time. Here we modified the model of Tatsumi et al. (1990) to emphasize the role of the stagnant Pacific slab in the formation of the intraplate volcanism in East Asia (Fig. 13).

Our results also suggest that the Longgang, Xianjindao, and Ch'Uga-Ryong volcanoes may have a similar cause and origin as the Changbai volcano because they are all located close to the Changbai volcano and there are low-velocity anomalies beneath them down to about 400-km depth (Figs. 10 and 11). Future efforts should be made to deploy portable seismic networks in these volcanic areas to determine the detailed 3-D mantle structure under the volcanoes to clarify their origins. At the same time, global and regional tomography models should be further improved to better understand the deep structure and dynamics of the NE Asia region.

Acknowledgements

We used the waveform data recorded by a portable seismic network installed by a research team led by Prof. F. T. Wu. We thank the IRIS Data Management Center for providing the waveform data used in this study. R. Engdahl provided the hypocentral parameters of the teleseismic events he relocated. M. Sambridge and X. Li provided the data for the geometry of the subducting Pacific slab in the present study area. The GMT software package distributed by Wessel and Smith (1995) was used for plotting the figures. This work is partially supported by grants from the Japan Society for the Promotion of Science (No. 11440134, No. 12002006). We thank Profs. E. Takahashi, T. Irifune, A. Yamada and M. Zhang for helpful discussions. We also thank the editors and two anonymous reviewers for their constructive comments and suggestions.

References

- Ai, Y., Zheng, T., Xu, W., He, Y., Dong, D., 2003. A complex 660 km discontinuity beneath northeast China. *Earth Planet. Sci. Lett.* 212, 63–71.

- Allen, R., Nolet, G., Morgan, W., Vogfjord, K., Bergsson, B., Erlendsson, P., Foulger, G., Jakobsdottir, S., Julian, B., Pritchard, M., Ragnarsson, S., Stefansson, R., 2002. Imaging the mantle beneath Iceland using integrated seismological techniques. *J. Geophys. Res.* 107, 2325.
- Basu, A., Wang, J., Huang, W., 1991. Major element, REE, and Pb, Nd and Sr isotropic geochemistry of Cenozoic volcanic rocks of eastern China: implications for their origin from suboceanic-type mantle reservoirs. *Earth Planet. Sci. Lett.* 105, 149–169.
- Dziewonski, A.M., Gilbert, F., 1976. The effect of small aspherical perturbations on travel times and a re-examination of the corrections for ellipticity. *Geophys. J. R. Astron. Soc.* 44, 7–17.
- Engdahl, E.R., van der Hilst, R.D., Buland, R., 1998. Global teleseismic earthquake relocation with improved travel times and procedures for depth determination. *Bull. Seismol. Soc. Am.* 88, 722–743.
- Fan, Q., Liu, R., Li, D., Li, Q., 1999a. Significance of K–Ar age of bimodal volcanic rocks at Wangtian's Volcano, Changbaishan area. *Chin. Sci. Bull.* 44, 660–663.
- Fan, Q., Liu, R., Wei, H., Sui, J., Li, N., 1999b. Petrogeochemical characteristics of Holocene eruption of the Tianchi Volcano, Changbai Mountains. *Geolog. Rev.* 45, 263–271 (Suppl.).
- Gudmundsson, O., Sambridge, M., 1998. A regionalized upper mantle (RUM) seismic model. *J. Geophys. Res.* 103, 7121–7136.
- Hetland, E., Wu, F., Song, J., 2004. Crustal structure in the Changbaishan volcanic area, China, determined by modeling receiver functions. *Tectonophysics* 386, 157–175.
- Inoue, T., Tanimoto, Y., Irfune, T., Suzuki, T., Fukui, H., Ohtaka, O., 2004. Thermal expansion of wadsleyite, ringwoodite, hydrous wadsleyite and hydrous ringwoodite. *Phys. Earth Planet. Inter.* 143–144, 279–290.
- Kennett, B.L.N., Engdahl, E.R., 1991. Traveltimes for global earthquake location and phase identification. *Geophys. J. Int.* 105, 429–465.
- Keyser, M., Ritter, J., Jordan, M., 2002. 3D shear-velocity structure of the Eifel plume, Germany. *Earth Planet. Sci. Lett.* 203, 59–82.
- Lei, J., Zhou, H., 2002. 3-D velocity structure of P wave in the upper mantle beneath southwestern China and its adjacent areas. *Acta Seismol. Sin.* 15 (2), 134–142.
- Li, X., Yuan, X., 2003. Receiver functions in northeast China—implications for slab penetration into the lower mantle in Northwest Pacific subduction zone. *Earth Planet. Sci. Lett.* 216, 679–691.
- Liu, R., 2000. Active Volcanoes in China. Seismological Press, Beijing, pp. 11–44.
- Paige, C.C., Saunders, M.A., 1982. LSQR: an algorithm for sparse linear equations and sparse least squares. *ACM Trans. Math. Softw.* 8, 43–71.
- Ritter, J., Jordan, M., Christensen, U., Achauer, U., 2001. A mantle plume below the Eifel volcanic fields, Germany. *Earth Planet. Sci. Lett.* 186, 7–14.
- Simkin, T., Siebert, L., 1994. Volcanoes of the world. Geoscience Press, Washington, DC, p. 111.
- Staudigel, H., King, S., 1992. Ultrafast subduction: the key to slab recycling efficiency and mantle differentiation? *Earth Planet. Sci. Lett.* 109, 517–530.
- Stein, S., Freymueller, J., 2002. Plate boundary zone. America Geophysical Union, Washington, DC, pp. 1–26.
- Sun, Y., Li, X., Kuleli, S., Morgan, F., Toksoz, M., 2004. Adaptive moving window method for 3D P-velocity tomography and its application in China. *Bull. Seismol. Soc. Am.* 94, 740–746.
- Tang, J., Liu, T., Jiang, Z., 1997. Preliminary observations of the Tianchi volcano area in Changbaishan Mountain by MT method. *Seismol. Geol.* 19 (2), 164–170.
- Tang, J., Jin, G., Zhao, G., 1999. Induction arrow and its application in Tianchi Volcano, Changbai Mountains. *Geolog. Rev.* 45, 294–303.
- Tang, J., Deng, Q., Zhao, G., 2001. Electric conductivity and magma chamber at the Tianchi volcano area in Changbaishan Mountain. *Seismol. Geol.* 23 (2), 191–200.
- Tatsumi, Y., Maruyama, S., Nohda, S., 1990. Mechanism of backarc opening in the Japan Sea: role of asthenospheric injection. *Tectonophysics* 181, 299–306.
- Thompsons, A., 1992. Water in the Earth's upper mantle. *Nature* 358, 295–302.
- Turcotte, D.L., Schubert, G., 1982. Geodynamics, Applications of Continuum Physics to Geological Problems. John Wiley and Sons press, New York, p. 44.
- Wang, Y., Li, C., Wei, H., Shan, X., 2003. Late Pliocene–recent tectonic setting for the Tianchi volcanic zone, Changbai Mountains, northeast China. *J. Asia Earth Sci.* 21, 1159–1170.
- Wessel, P., Smith, W., 1995. New version of the Generic Mapping Tools (GMT) version 3.0 released. *EOS Trans. AGU* 76, 329.
- Wolfe, C., Bjarnason, I., VanDecar, J., Solomon, S., 1997. Seismic structure of the Iceland mantle plume. *Nature* 385, 245–247.
- Wu, F., Hetland, E., 1999. The Changbaishan, China, PASSCAL experiment. 21st Seismic Research Symposium: Technologies for Monitoring the Comprehensive Nuclear-Test-Ban Treaty, Las Vegas, NV, USA.
- Yin, A., 2000. Mode of Cenozoic east–west extension in Tibet suggesting a common origin of rifts in Asia during the Indo-Asian collision. *J. Geophys. Res.* 105, 21745–21760.
- Zhang, M., O'Reilly, S., 1997. Geochemical evolution of basaltic rocks from the Changbai Mountains: implications for the nature of lithospheric mantle beneath the NE margin of the Sino-Korean craton. In: Lee, Y., Kim, J. (Eds.), *Tectonic Evolution of Eastern Asian Continent*, Geol. Soc. Korea 50th Anniv. Int'l. Symp., pp. 170–175.
- Zhang, L., Tang, X., 1983. Subduction of the west Pacific Plate and deep-source seismic zone in northeast China. *Acta Geophys.* 26, 331–340.
- Zhang, C., Zhang, X., Zhao, J., Liu, B., Zhang, J., Yang, Z., Hai, Y., Sun, G., 2002. Crust–mantle structure of the Changbaishan Tianchi volcanic region and its vicinity: an exploratory study and inferences. *Chin. J. Geophys.* 45 (6), 862–871.
- Zhao, Z., 1991. Characteristics of intermediate and deep earthquakes in and near Japan Sea. *Northeast. Seismol. Res.* 4, 37–43.
- Zhao, D., 2001a. Seismic structure and origin of hotspots and mantle plumes. *Earth Planet. Sci. Lett.* 192, 251–265.
- Zhao, D., 2001b. Seismological structure of subduction zone and its implications for arc magmatism and dynamics. *Phys. Earth Planet. Inter.* 127, 197–214.

- Zhao, D., 2004. Global tomographic images of mantle plumes and subducting slabs: insight into deep Earth dynamics. *Phys. Earth Planet. Inter.* 146, 3–34.
- Zhao, D., Lei, J., 2004. Seismic ray path variations in a 3-D global velocity model. *Phys. Earth Planet. Inter.* 141, 153–166.
- Zhao, D., Hasegawa, A., Horiuchi, S., 1992. Tomographic imaging of P and S wave velocity structure beneath northeastern Japan. *J. Geophys. Res.* 97, 19909–19928.
- Zhao, D., Hasegawa, A., Kanamori, H., 1994. Deep structure of Japan subduction zone as derived from local, regional, and teleseismic events. *J. Geophys. Res.* 99, 22313–22329.
- Zhao, D., Xu, Y., Wiens, D., Dorman, L., Hildebrand, J., Webb, S., 1997. Depth extent of the Lau back-arc spreading center and its relation to subduction processes. *Science* 278, 254–257.
- Zindler, A., Hart, S., 1986. Chemical geodynamics. *Annu. Rev. Earth Planet. Sci.* 14, 463–471.